

---

# A Guide to Integrating Sphere Theory and Applications



T  
E  
C  
H  
N  
I  
C  
A  
L  
G  
U  
I  
D  
E

**TABLE OF CONTENTS**

- 1.0 Integrating Sphere Theory ..... 2-5
  - 1.1 Radiation Exchange Within a Spherical Enclosure ..... 2
  - 1.2 The Integrating Sphere Radiance Equation ..... 3
    - 1.2.1 The Sphere Multiplier ..... 4
    - 1.2.2 The Average Reflectance ..... 4
  - 1.3 Spatial Integration ..... 4
  - 1.4 Temporal Response of an Integrating Sphere ..... 5
- 2.0 Integrating Sphere Design ..... 6-9
  - 2.1 Integrating Sphere Diameter ..... 6
  - 2.2 Integrating Sphere Coating Selection ..... 6
  - 2.3 Baffles and Detector Field-of-View ..... 7
  - 2.4 Flux on the Photodetector ..... 8
  - 2.5 Fiberoptic Coupling ..... 9
- 3.0 Integrating Sphere Applications ..... 10-17
  - 3.1 Radiometers and Photometers ..... 10
    - 3.1.1 The Sphere Photometer ..... 10
    - 3.1.2 Laser Power Meters ..... 11
    - 3.1.3 Cosine Receptor ..... 11
  - 3.2 Reflectance and Transmittance of Materials ..... 12
    - 3.2.1 Substitution vs. Comparison Spheres ..... 13
    - 3.2.2 Measurement Geometry  $0^\circ/d$  vs.  $d/0^\circ$  ..... 14
  - 3.3 Uniform Sources ..... 15
    - 3.3.1 Modifying the Source Radiance ..... 16
    - 3.3.2 Irradiance Uniformity ..... 16

1.0 Integrating Sphere Theory

The integrating sphere is a simple, yet often misunderstood device for measuring optical radiation. The function of an integrating sphere is to spatially integrate radiant flux. Before one can optimize a sphere design for a particular application, it is important to understand how the integrating sphere works. How light passes through the sphere begins with a discussion of diffuse reflecting surfaces. From this, the radiance of the inner surface of an integrating sphere is derived and two related sphere parameters are discussed, the sphere multiplier and the average reflectance. Finally, the time constant of an integrating sphere as presented is relevant to applications involving fast pulsed or short lived radiant energy.

1.1 Radiation Exchange Within a Spherical Enclosure

The theory of the integrating sphere originates in the theory of radiation exchange within an enclosure of diffuse surfaces. Although the general theory can be rather complex, the sphere is a unique, yet simple solution to understand.

Consider the radiation exchange between two differential elements of diffuse surfaces.

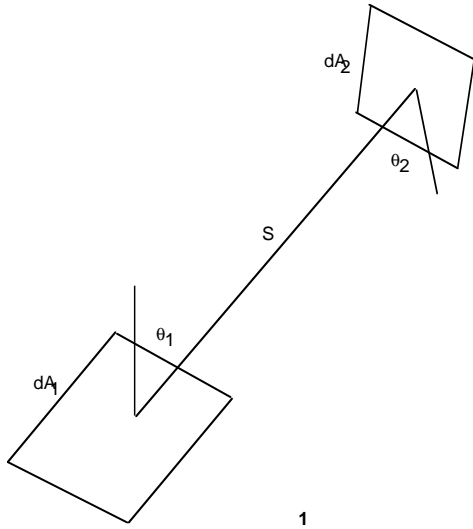


FIGURE 1

The fraction of energy leaving  $dA_1$  and arriving at  $dA_2$  is known as the exchange factor  $dF_{d_1-d_2}$ . It is given by:

$$dF_{d_1-d_2} = \frac{\cos \theta_1 \cos \theta_2}{\pi S^2} dA_2 \tag{EQ. 1}$$

Where  $\theta_1$  and  $\theta_2$  are measured from the surface normals.

Consider two differential elements,  $dA_1$  and  $dA_2$  inside a diffuse surface sphere.

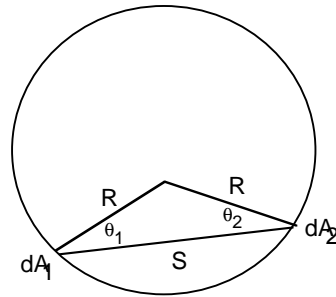


FIGURE 2

Since the distance  $S = 2R \cos \theta_1 = 2R \cos \theta_2$ ;

$$dF_{d_1-d_2} = \frac{dA_2}{4\pi R^2} \tag{EQ.2}$$

The result is significant since it is independent of viewing angle and the distance between the areas. Therefore, the fraction of flux received by  $dA_2$  is the same for any radiating point on the sphere surface.

If the infinitesimal area  $dA_1$  instead exchanges radiation with a finite area  $A_2$ , then Eq. 2 becomes:

$$dF_{d_1-d_2} = \frac{1}{4\pi R^2} \int_{A_2} dA_2 = \frac{A_2}{4\pi R^2} \tag{EQ. 3}$$

Since this result is also independent of  $dA_1$  :

$$F_{1-2} = \frac{A_2}{4\pi R^2} = \frac{A_2}{A_s} \tag{EQ. 4}$$

Where  $A_s$  is the surface area of the entire sphere. Therefore, the fraction of radiant flux received by  $A_2$  is the fractional surface area it consumes within the sphere.

# INTEGRATING SPHERE THEORY AND APPLICATIONS

## 1.2 The Integrating Sphere Radiance Equation

Light incident on a diffuse surface creates a virtual light source by reflection. The light emanating from the surface is best described by its *radiance*, the flux density per unit solid angle. Radiance is an important engineering quantity since it is used to predict the amount of flux that can be collected by an optical system that might view the illuminated surface.

Deriving the radiance of an internally illuminated integrating sphere begins with an expression of the radiance,  $L$ , of a diffuse surface for an input flux,  $\Phi_i$ .

$$L = \frac{\Phi_i \rho}{\pi A} \quad (\text{W/m}^2/\text{sr}) \quad \text{EQ. 5}$$

Where  $\rho$  is the reflectance,  $A$  the illuminated area and  $\pi$  the total projected solid angle from the surface.

For an integrating sphere, the radiance equation must consider both multiple surface reflections and losses through the port openings needed to admit the input flux,  $\Phi_i$ , as well as view the resulting radiance. Consider a sphere with input port area  $A_i$  and exit port  $A_e$ .

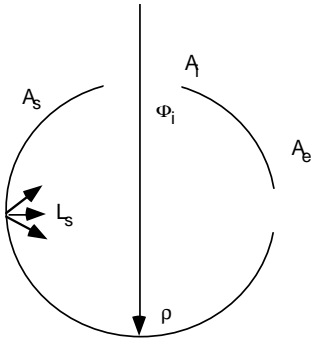


FIGURE 3

The input flux is perfectly diffused by the initial reflection. The amount of flux incident on the entire sphere surface is:

$$= \Phi_i \rho \left( \frac{A_s - A_i - A_e}{A_s} \right) \quad \text{EQ. 6}$$

Where the quantity in parenthesis denotes the fraction of flux received by the sphere surface that is not consumed by the port openings. It is more convenient to write this term as  $(1-f)$  where  $f$  is the port fraction and  $f = (A_i + A_e)/A_s$ . When more than two ports exist,  $f$  is calculated from the sum of all port areas.

By similar reasoning, the amount of flux incident on the sphere surface after the second reflection is:

$$= \Phi_i \rho^2 (1-f)^2 \quad \text{EQ. 7}$$

The third reflection produces an amount of flux equal to

$$= \Phi_i \rho^3 (1-f)^3 \quad \text{EQ. 8}$$

It follows that after  $n$  reflections, the total flux incident over the entire integrating sphere surface is:

$$\Phi_i \rho (1-f) \{1 + \rho(1-f) + \dots + \rho^{n-1}(1-f)^{n-1}\} \quad \text{EQ. 9}$$

Expanding to an infinite power series, and given that  $\rho(1-f) < 1$ , this reduces to a simpler form:

$$= \frac{\Phi_i \rho (1-f)}{1 - \rho(1-f)} \quad (\text{WATTS}) \quad \text{EQ. 10}$$

Equation 10 indicates that the total flux incident on the sphere surface is higher than the input flux due to multiple reflections inside the cavity. It follows that the sphere surface radiance is given by:

$$L_s = \frac{\Phi_i}{\pi A_s (1-f)} * \frac{\rho(1-f)}{1 - \rho(1-f)} \quad \text{EQ. 11}$$

$$= \frac{\Phi_i}{\pi A_s} * \frac{\rho}{1 - \rho(1-f)} \quad \text{EQ. 12}$$

This equation is used to predict integrating sphere radiance for a given input flux as a function of sphere diameter, reflectance, and port fraction. Note that the radiance decreases as sphere diameter increases.

1.2.1 The Sphere Multiplier

Equation 12 is purposely divided into two parts. The first part is approximately equal to Eq. 5, the radiance of a diffuse surface. The second part of the equation is a unitless quantity which can be referred to as the sphere multiplier.

$$M = \frac{\rho}{1 - \rho(1 - f)} \quad \text{EQ. 13}$$

It accounts for the increase in radiance due to multiple reflections. The following chart illustrates the magnitude of the sphere multiplier,  $M$ , and its strong dependence on both the port fraction,  $f$  and the sphere surface reflectance  $\rho$ .

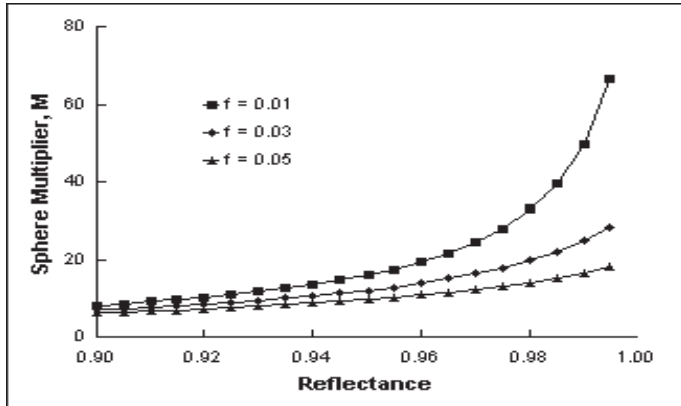


FIGURE 4

A simplified intuitive approach to predicting a flux density inside the integrating sphere might be to simply divide the input flux by the total surface area of the sphere. However, the effect of the sphere multiplier is that the radiance of an integrating sphere is at least an order of magnitude greater than this simple intuitive approach. A handy rule of thumb is that for most real integrating spheres ( $.94 < \rho < .99$ ;  $.02 < f < .05$ ), the sphere multiplier is in the range of 10 - 30.

1.2.2 The Average Reflectance

The sphere multiplier in Eq. 13 is specific to the case where the incident flux impinges on the sphere wall, the wall reflectance is uniform and the reflectance of all port areas is zero. The general expression is:

$$M = \frac{\rho_0}{1 - \rho_w \left( 1 - \sum_{i=0}^n f_i \right) - \sum_{i=0}^n \rho_i f_i} \quad \text{EQ. 14}$$

where;  $\rho_0$  = the initial reflectance for incident flux

$\rho_w$  = the reflectance of the sphere wall

$\rho_i$  = the reflectance of port opening  $i$

$f_i$  = the fractional port area of port opening  $i$

The quantity  $\rho_w \left( 1 - \sum_{i=0}^n f_i \right) + \sum_{i=0}^n \rho_i f_i$  can also be described as the average reflectance  $\bar{\rho}$  for the entire integrating sphere. Therefore, the sphere multiplier can be rewritten in terms of both the initial and average reflectance:

$$M = \frac{\rho_0}{1 - \bar{\rho}} \quad \text{EQ. 15}$$

1.3 Spatial Integration

An exact analysis of the distribution of radiance inside an actual integrating sphere would depend on the distribution of incident flux, the geometrical details of the actual sphere design, and the reflectance distribution function for the sphere coating as well as each surface of each device mounted at a port opening or inside the integrating sphere. Design guidelines for optimum spatial performance are based on maximizing both the coating reflectance and the sphere diameter with respect to the required port openings and system devices.

The effect of the reflectance and port fraction on the spatial integration can be illustrated by considering the number of reflections required to achieve the total flux incident on the sphere surface given by Eq. 10. The total flux on the sphere wall after only  $n$  reflections can be written as:

$$= \Phi_i \sum_{n=1}^n \rho^n (1 - f)^n \quad \text{EQ. 16}$$

The radiance produced after only  $n$  reflections can be compared to the steady state condition.

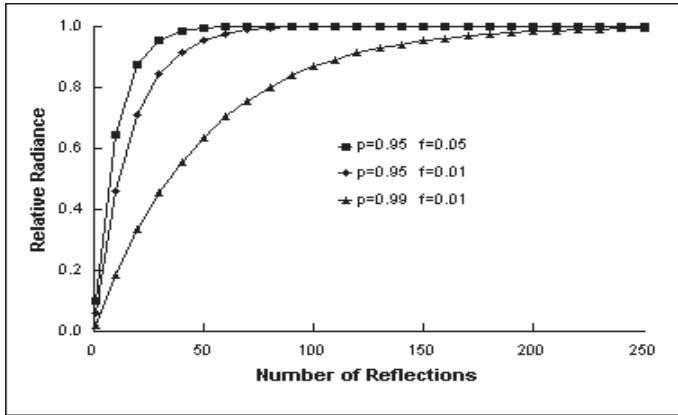


FIGURE 5

Since the integrating sphere is most often used in the steady state condition, a greater number of reflections produces the steady state radiance as both  $\rho$  increases and  $f$  decreases. Therefore, integrating sphere designs should attempt to optimize both parameters for the best spatial integration of radiant flux.

## 1.4 Temporal Response of an Integrating Sphere

Most integrating spheres are used as steady state devices. The previous analysis of their performance and application assumes that the light levels within the sphere have been constant for a long enough time so that all transient response has disappeared. If rapidly varying light signals, such as short pulses or those modulated at high (radio) frequencies, are introduced into an integrating sphere, the output signal may be noticeably distorted by the “pulse stretching” caused by the multiple diffuse reflections. The shape of the output signal is determined by convolving the input signal with the impulse response of the integrating sphere.

This impulse response is of the form:

$$e^{-t/\tau} \quad \text{EQ. 17}$$

where the time constant,  $\tau$ , is calculated as:

$$\tau = -\frac{2}{3} \cdot \frac{D_s}{c} \cdot \frac{1}{\ln \bar{\rho}} \quad \text{EQ. 18}$$

and  $\bar{\rho}$  = the average wall reflectance  
 $c$  = the velocity of light  
 $D_s$  = the diameter of the integrating sphere

Time constants of typical integrating spheres range from a few nanoseconds to a few tens of nanoseconds.

2.0 Integrating Sphere Design

The design of an integrating sphere for any application involves a few basic parameters. This includes selecting the optimum sphere diameter based on the number and size of port openings and peripheral devices. Selecting the proper sphere coating considers spectral range as well as performance requirements. The use of baffles with respect to incident radiation and detector field-of-view is discussed; and radiometric equations are presented for determining the coupling efficiency of an integrating sphere to a detection system.

2.1 Integrating Sphere Diameter

Figure 4 indicates that decreasing the port fraction has a dramatic effect on increasing the sphere multiplier. For port fractions larger than 0.05, one begins to lose the advantage offered by the high reflectance coatings available for integrating spheres. The first rule of thumb for integrating spheres is that no more than 5% of the sphere surface area be consumed by port openings.

Real integrating spheres are designed by initially considering the diameter required for the port openings. Port diameter is driven by both the size of devices as well as the geometrical constraints required by a sphere system.

Consider the case of a two port integrating sphere; both ports are of unit diameter. The relative radiance produced as a function of sphere diameter,  $D_s$ , for an equivalent input flux is proportional to:

$$L_s \propto \frac{M}{D_s^2} \tag{EQ. 19}$$

The equation can be plotted as a function of reflectance for different sphere diameters and the resulting port fraction for each is shown in Figure 6.

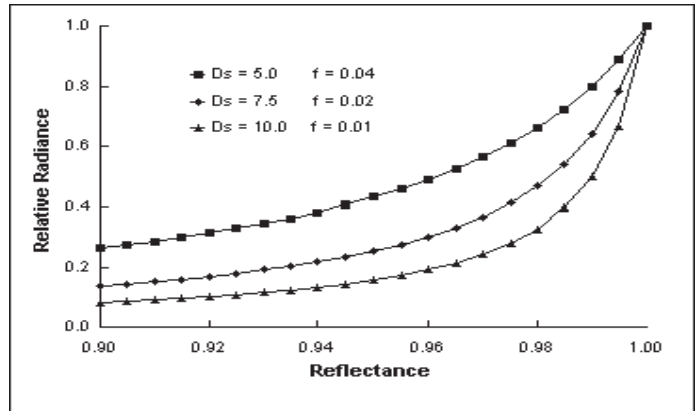


FIGURE 6

The smallest sphere produces the highest radiance in general. However, since the integrating sphere is usually employed for its ability to spatially integrate input flux, a larger sphere diameter and smaller port fraction will improve the spatial performance. Notice in Figure 6 that all three sphere designs converge on the same unit flux density as the reflectance approaches 1.0. Therefore, high reflectance integrating sphere materials such as Spectralon can optimize spatial performance at only a slight tradeoff in radiance efficiency.

2.2 Integrating Sphere Coating Selection

The sphere multiplier as illustrated by Figure 4 is extremely sensitive to the sphere surface reflectance. Therefore, the selection of sphere coating or material can make a large difference in the radiance produced for a given sphere design. Consider the diffuse reflectors offered by Labsphere known as Spectralect and Spectralon. Both are useful for UV-VIS-NIR applications in the 250 nm to 2500 nm spectral region. The typical spectral reflectance of each is shown in Figure 7 below.

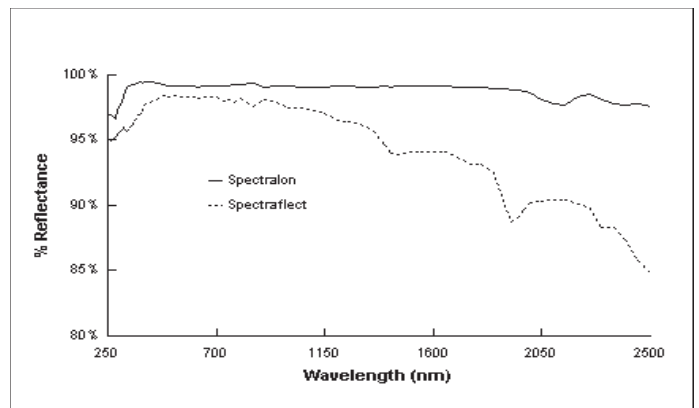


FIGURE 7

# INTEGRATING SPHERE THEORY AND APPLICATIONS

Both coatings are highly reflective, over 95% from 350 nm to 1350 nm, therefore, intuitively one might expect no significant increase in radiance for the same integrating sphere. However, the relative increase in radiance is greater than the relative increase in reflectance by a factor equal to the new sphere multiplier,  $M_{new}$ .

$$\frac{\Delta L_s}{L_s} \approx \frac{\Delta \rho}{\rho_0} * M_{new} \quad \text{EQ. 20}$$

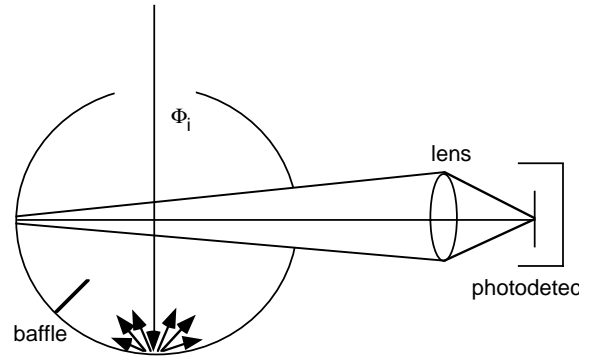


FIGURE 9

The magnitude of this effect is depicted below:

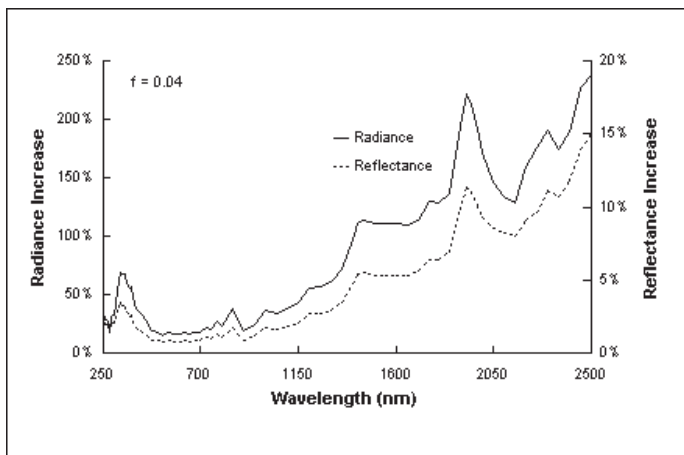


FIGURE 8

Although Spectralon offers a 2% to 15% increase in reflectance over Spectralect within the wavelength range, an identical integrating sphere design would offer 40% to 240% increased radiance. The largest increase occurs in the NIR spectral region above 1400 nm.

## 2.3 Baffles and Detector Field-of-View

In using integrating spheres, it is important that the viewed radiance does not include a portion of the sphere surface directly irradiated by incident flux. This will introduce a false response.

Baffles coated with the same material as the integrating sphere wall block the view of incident flux which has not undergone at least two reflections from the sphere surface. The optical system in Figure 9 cannot directly view the incident flux. However, the baffle is positioned to prevent first reflections from entering the field-of-view for the photodetector.

Baffles can be considered extensions of the sphere surface. Their contribution to the sphere area can be factored into the radiance equation although it is not usually significant. The fractional contribution of baffles to the sphere surface area is usually quite small.

The radiance at the incident area,  $L_i$  is higher than the average for the entire sphere surface by an amount equal to Eq. 5 for the directly irradiated area  $A_i$ . The radiance ratio for the incident to average sphere radiance is given by:

$$\frac{L_i}{L_s} = 1 + \frac{1 - \bar{\rho}}{f_i} \quad \text{EQ. 21}$$

where  $f_i = A_i/A_s$

The radiance ratio increases rapidly with decreasing spot diameter. Considering the reciprocity of light rays, the same considerations must be applied to the field-of-view of a photodetector within the integrating sphere. The fractional area  $f_i$  can be converted into the detector's angular field-of-view.

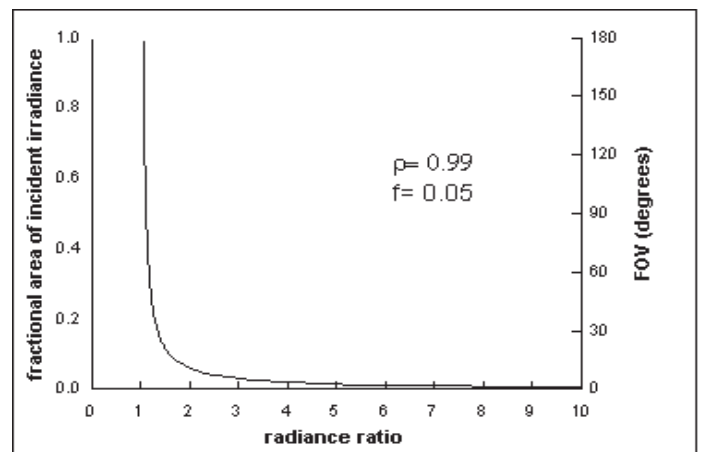


FIGURE 10



In both cases, as either the area of irradiation or the field-of-view approaches total coverage of the sphere surface, the radiance ratio approaches unity. As either parameter decreases, the radiance ratio rapidly increases. In applications where the port of an integrating sphere is being used as a uniform radiance source, the result is increased non-uniformity. When the sphere is used as a collector to measure radiant flux, the result is increased measurement error if incident flux directly enters the detector's field-of-view.

One method of providing a photodetector with a hemispherical field-of-view is to attach a diffuser. One of the best diffuser attachments is an auxiliary or satellite integrating sphere. The port of this sphere is baffled from direct view of incident flux.

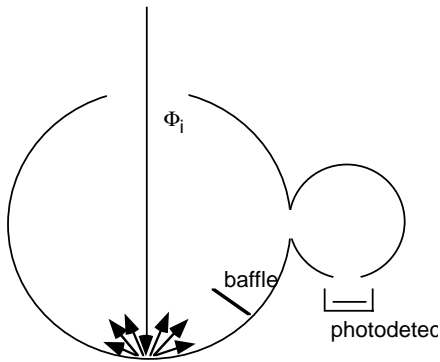


FIGURE 11

Of course, Figure 9 (on the previous page) presents another solution to the potential problem of small detector field-of-view. In this case, the real field-of-view on the sphere wall as defined by the photodetector's imaging system can be considered as a "virtual detector" with a hemispherical field-of-view. The baffle placement ensures this effect. The integrating sphere applications shown in Section 3.0 present other examples of proper baffle placement.

2.4 Flux on the Photodetector

The radiance of the sphere wall determines the total flux incident on a photodetector mounted at or near a port of the integrating sphere.

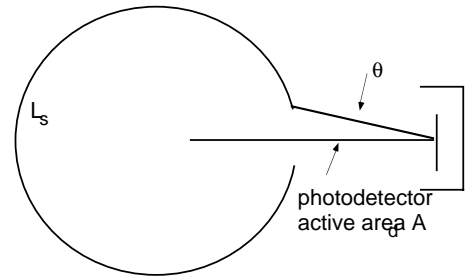


FIGURE 12

By definition, the total flux incident on the detector active area,  $A_d$  ( $m^2$ ) is:

$$\Phi_d = L_s A_d \Omega \quad (\text{WATTS}) \quad \text{EQ. 22}$$

where:  $\Omega$  = projected solid angle ( $sr$ )

A good approximation for  $\Omega$  in almost all cases is:

$$\Omega = \pi \sin^2 \theta \quad (sr) \quad \text{EQ. 23}$$

In the case of imaging optics used with the detector, the angle  $\theta$  is subtended from the exit pupil of the system. The detector is the field stop of the system.

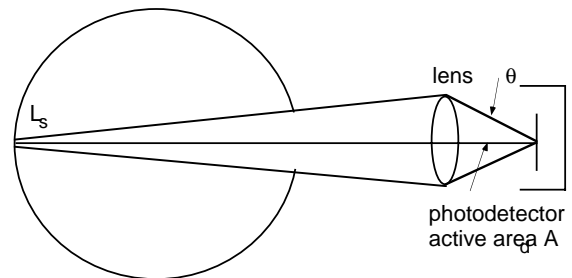


FIGURE 13

## INTEGRATING SPHERE THEORY AND APPLICATIONS

The f-number ( $f/\#$ ) of an optical system is also used to express its light gathering power. Therefore:

$$\Omega = \frac{\pi}{(2 f/\#)^2} \quad (\text{WATTS}) \quad \text{EQ. 24}$$

The efficiency of the optical system, which is generally a function of the transmittance and reflectance of individual components, must also be considered. Therefore the detector incident flux is:

$$\Phi_d = L_s A_d \frac{\pi}{(2 f/\#)^2} \epsilon_0 \quad (\text{sr}) \quad \text{EQ. 25}$$

where,  $\epsilon_0$  = optical system efficiency (unitless).

### 2.5 Fiberoptic Coupling

A similar equation is used to calculate the incident flux gathered by a fiberoptic cable coupled to an integrating sphere.

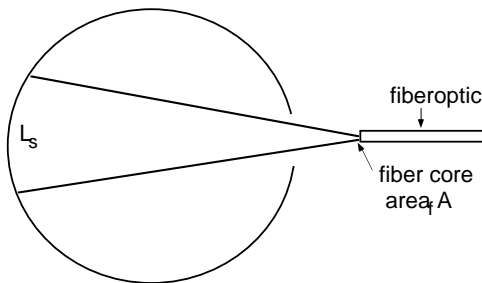


FIGURE 14

The numerical aperture (NA) of an optical fiber is used to describe its light coupling ability. The projected solid angle is:

$$\Omega = \pi(NA)^2 \quad (\text{sr}) \quad \text{EQ. 26}$$

Reflectance losses at the air/fiber interface must be considered in determining the total flux accepted by the fiber. If  $R$  is the reflectance at the fiber face, then:

$$\Phi_f = L_s A_f \pi (NA)^2 (1 - R) \quad (\text{WATTS}) \quad \text{EQ. 27}$$

For a single strand fiber,  $A_f$  is the area of the fiber end calculated for the core diameter. If a fiber bundle is used, this quantity becomes the individual core diameter times the number of fibers in the bundle. The light emanating from the other end of the fiber is a function of its length (cm), the material extinction coefficient ( $\text{cm}^{-1}$ ), and the exit interface reflection.

### 3.0 Integrating Sphere Applications

Integrating spheres collect and spatially integrate radiant flux. The flux can be measured directly or after it has interacted with a material sample. The sphere as part of a radiometer or photometer can directly measure the flux originating from lamps and lasers or the flux density produced from hemispherical illumination. Perhaps the largest application for integrating spheres is in the measurement of the total reflectance or transmittance from diffuse or scattering materials. An alternative application utilizes the port opening of an internally illuminated integrating sphere as a large area source that features uniform radiance. These sources can be used to calibrate electronic imaging devices and systems or simply as uniform back illuminators.

#### 3.1 Radiometers and Photometers

An integrating sphere combined with a photodetector of the appropriate spectral response can be used to directly measure the total geometric flux emanating from a light source or the flux density of an illuminated area. The geometric distribution of the light to be measured determines the appropriate integrating sphere design. The spectral properties of the light source determines the appropriate photodetection system.

In general, radiometers measure light in accordance with the SI unit of radiant flux, the watt. Quantum response photodetectors are most commonly used in radiometers. Since their responsivity varies spectrally, it is more appropriate to tailor the response for a specific spectral region through the use of optical filters in nearly all cases except perhaps when the incident flux is monochromatic.

Thermal detectors respond equally to all wavelengths of light. This property also makes them susceptible to background thermal radiation. Most often, they need to be temperature controlled and the input radiation is modulated for synchronous detection.

Spectroradiometers measure light as a function of wavelength. These feature a detector coupled to a spectral separation device such as a diffraction grating monochromator or a Fourier transform interferometer.

The spectral dependence of the integrating sphere multiplier modifies the relative spectral responsivity of the photodetector. The sphere/detector combination must be considered mutually in order to design or calibrate the measurement system for a particular responsivity.

Photometers are a distinct type of radiometer which use a quantum detector filtered to emulate the spectral response of the standard human observer. This specific responsivity is known as the luminous efficiency function. The primary unit of photometric flux is the lumen. The detector response function weights and integrates the spectral radiant flux to produce the lumen scale. Photometry has the unique distinction of being the only system of physical measurement based entirely on human perception.

#### 3.1.1 The Sphere Photometer

The oldest application for the integrating sphere is the measurement of total geometric luminous flux from electric lamps. The technique originated at the turn of the 20th century as a simple and fast method of comparing the lumen output of different lamp types. It is still widely used in the lamp industry for manufacturing quality control. The alternative method is a goniophotometer which would need to rotate a photodetector in a complete sphere around the lamp. Each discrete intensity point ( $\text{lm/sr}$ ) is then integrated over  $4\pi$  steradians.

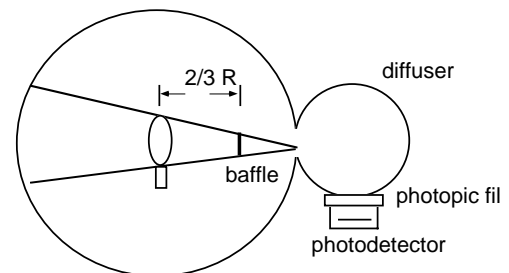


FIGURE 15

In a sphere photometer, the lamp to be measured is mounted at the center of the integrating sphere and baffled from the viewing port equipped with a diffuser and photopic response detector. The baffle is usually positioned at  $2/3$  of the radius of the sphere center. Its size should be as small as possible yet large enough to screen the maximum dimension of the lamp.

The lumen output from the test lamp is determined by first calibrating the photodetector signal using a lamp standard of known luminous flux. The lamps are alternately substituted into the integrating sphere. An auxiliary lamp can be permanently mounted inside the sphere to correct for the substitution error caused by different self absorption from the test and standard lamps. Auxiliary lamps are

usually mounted at the sphere vertex diametrically opposite the viewing port. Lamp standards originate from national standardizing laboratories and are based on goniophotometric measurements.

The photopic response detector in Figure 15 can be replaced with a spectroradiometer for direct measurements of spectral radiant flux. The ability to obtain spectral information from the integrating sphere is advantageous for several reasons. With spectral measurements, the spectral responsivity of the sphere wall and the relative spectral responsivity of the photodetector do not influence the luminous efficiency function. Lumens is not the only quantity obtained for a particular lamp. Spectral flux is easily converted to yield important color properties such as chromaticity coordinates, correlated color temperature, and the color rendering indices.

### 3.1.2 Laser Power Meters

The sphere photometer offers the advantage of total collection and spatial integration. In the measurement of highly collimated sources such as lasers, the integrating sphere offers the advantage of signal attenuation. From Eq. 12 and Eq. 22, it is evident that the fraction of flux received by a photodetector mounted at the sphere surface is approximately the fractional surface area consumed by its active area times the sphere multiplier.

For a  $1\text{mm}^2$  active area on a  $100\text{mm}$  diameter sphere, the detected flux would be less than 0.1% of the incident flux. Even further attenuation is possible by recessing the detector from the sphere port as in Figure 12.

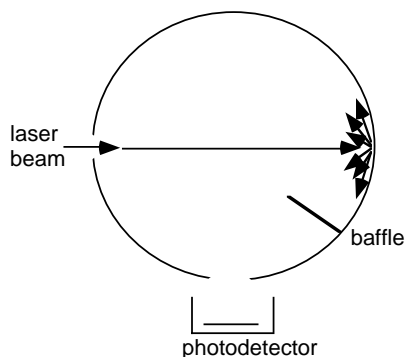


FIGURE 16

The attenuation and insensitivity to misalignment provides a laser power meter which employs a photodetector with a smaller and faster active area. Integrating sphere power

meters have been used to measure industrial CW lasers at kilowatt levels. The high reflectance of the integrating sphere coating avoids direct damage from the first strike. The utilization of faster response detectors supports real time power monitoring in feedback control of industrial laser output.

Integrating sphere power meters are extremely useful for divergent and non-symmetrical beams such as those produced by diode lasers. These tend to overfill the active area of conventional laser power meters. Except in the case of high power diode laser arrays, the integrating sphere is once again utilized more for its ability to spatially integrate radiant flux than its ability to attenuate.

The baffle placement should be based on preventing direct view of the "hot spot" produced by the laser beam as depicted in Figure 16.

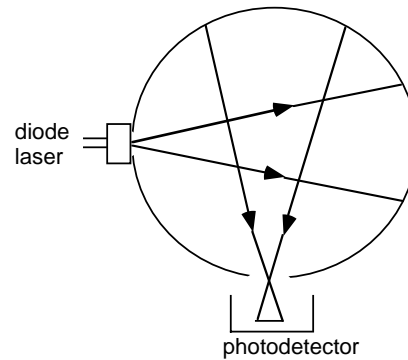


FIGURE 17

In the case of diode lasers, the field-of-view of the detector should not overlap the direct area of illumination. Although the design tendency in this application may be to select a small sphere diameter to coincide with the device dimensions, a larger diameter sphere more easily conforms to the geometrical requirements and reduces the measurement uncertainty.

### 3.1.3 Cosine Receptor

In the sphere photometer and laser power meter examples, the integrating sphere is used for measuring total radiant flux. The geometry of the radiant source in both applications takes advantage of total flux collection by the sphere. In the measurement of flux density, photodetectors by themselves do not exhibit uniform response. Diffusers are usually attached to provide the needed uniformity. The integrating sphere is one such diffuser.

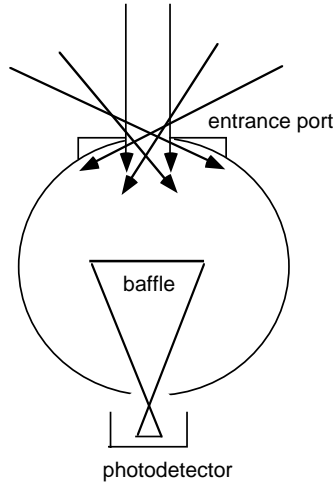


FIGURE 18

The centrally located baffle prevents direct irradiation of the detector. The entrance port becomes the effective measuring aperture of the device. For regular irradiance measurements, the cosine angular response is required. The irradiance of a flat surface  $E$ , is proportional to the cosine of the angle of incidence,  $\theta$ .

$$E(\theta) = E(0)\cos \theta \quad \text{EQ. 28}$$

For spectral irradiance measurements in which a monochromator is used, a  $90^\circ$  port geometry can be more accommodating. This design is commonly used for global irradiance monitors since the integrating sphere provides good spectral response from the UV to the NIR regions of the atmospheric solar spectrum. A quartz weather dome guards against environmental contaminants.

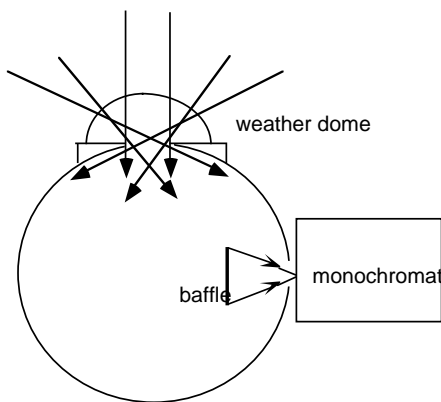


FIGURE 19

In either design, the angular response does not perfectly correspond to the cosine function since certain incident rays will first impose on the baffle before being distributed to the sphere wall. The true angular response is usually determined experimentally and then applied as a correction factor in high accuracy irradiance measurements.

### 3.2 Reflectance and Transmittance of Materials

The single largest application for integrating spheres is the measurement of the reflectance and transmittance of diffuse or scattering materials. The measurements are almost always performed spectrally, as a function of wavelength. The one exception may be the measurement of luminous reflectance or transmittance using a photopic response detector.

In the ultraviolet, diffuse transmittance is used to determine the UV resistance of pharmaceutical containers, sun protective clothing, and automotive paints. In the visible spectrum, the color of materials is quantified and controlled in industries such as paints, textiles and the graphic arts. In the infrared, the total hemispherical reflectance determines surface emissivities applied to radiant heat transfer analysis of thermal control coatings and foils used in spacecraft design.

A transmittance measurement places a material sample at the entrance port to the sphere (as shown in Figure 20).

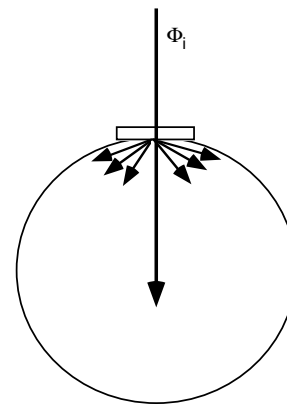


FIGURE 20

In reflectance measurements, the sample is placed at a port opening opposite the entrance port. The incident flux is reflected by the sample. The total hemispherical reflectance, both the diffuse and specular components, is collected by the integrating sphere.

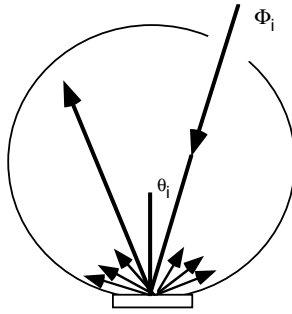


FIGURE 21

The angle of incidence in reflectance measurements is usually slightly off normal up to 10°. The specular component can be excluded from the measurement by using normal (0°) incidence or by fitting another port in the specular path and using a black absorbing light trap to extinguish the specular flux.

Reflectance measurements at larger or variable incident angles are performed by placing the sample at the center of the sphere and rotating it about a fixed input beam.

Baffles are placed to prevent the photodetector on the sphere from directly viewing the irradiated sample in either measurement. In the reflectance geometry, a baffle is usually placed between the portion of the sphere wall that receives the specular component as well. It is best to use a photodetector with a hemispherical field-of-view to reduce any sensitivity to the scatter distribution function of the sample.

### 3.2.1 Substitution vs. Comparison Spheres

A unique integrating sphere error is attributed to the designs depicted in Figure 20 and Figure 21 due to the sample effectively altering the average reflectance of the sphere wall. Calibration of the transmittance scale is usually performed by initially measuring the incident flux before the sample is placed against the entrance port.

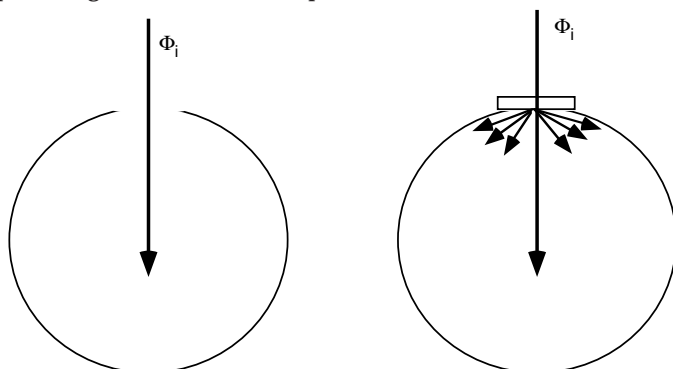


FIGURE 22

Calibration of the reflectance scale is performed by comparing the incident flux remaining in the sphere after reflecting from a standard reference material.

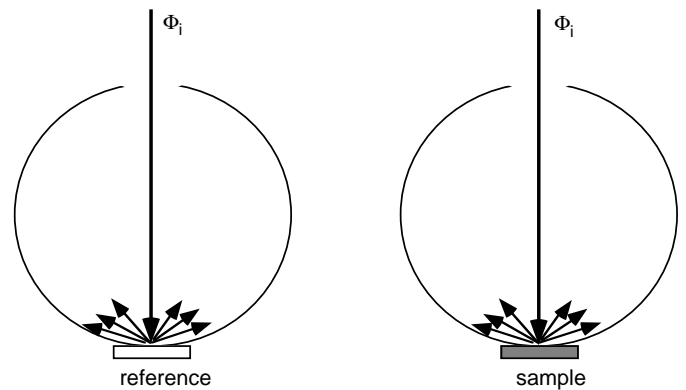


FIGURE 23

The ideal measurement relationship is for the ratio of radiance produced inside the sphere to be equal to the ratio of the reflectance for each material.

$$\frac{L_s}{L_r} = \frac{\rho_s}{\rho_r} \quad \text{EQ. 29}$$

where;  $\rho_r$  = the reflectance of the reference material

The sample measurement quantity,  $\rho_s$  is properly known as the *reflectance factor*. The term refers to the fact that the incident flux was not directly measured as the reference.

However, in the *substitution sphere* of Figure 23, the average reflectance of the sphere changes when the sample is substituted for the reference material. The true measurement equation in a substitution sphere is, therefore;

$$\frac{L_s}{L_r} = \frac{\rho_s}{\rho_r} \cdot \frac{1 - \bar{\rho}_r}{1 - \bar{\rho}_s} \quad \text{EQ. 30}$$

where;  $\bar{\rho}_s$  = average wall reflectance with sample

$\bar{\rho}_r$  = average wall reflectance with reference

The average reflectance with the sample material in place,  $\bar{\rho}_s$  cannot be easily determined since it is also dependent on  $\rho_s$ . The magnitude of this error can be plotted for a typical Spectrafect integrating sphere with 5% port openings and a 1% sample port opening. The reference material is Spectralon.

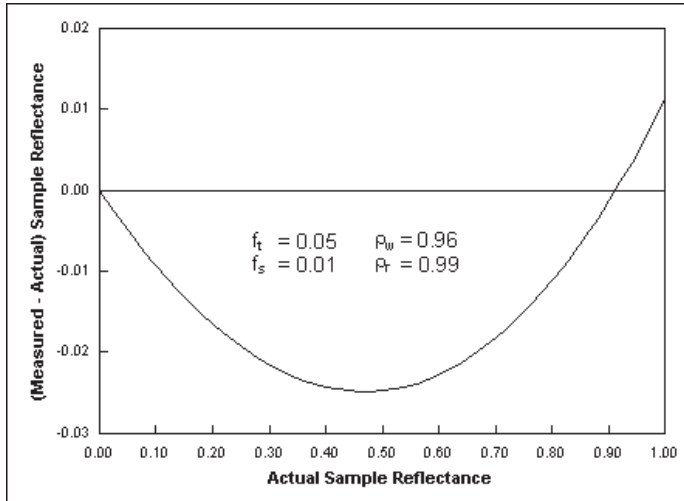


FIGURE 24

In order to utilize Eq. 29, the proper sphere design is one that keeps the average reflectance constant. A *comparison sphere* mounts both the sample and the reference simultaneously to port openings in the integrating sphere.

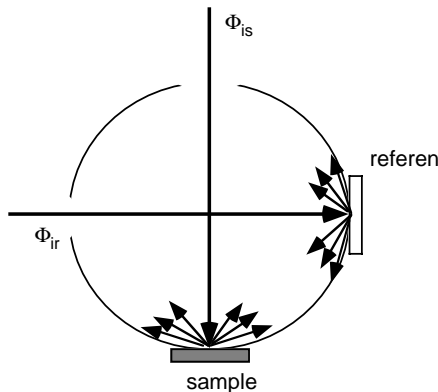


FIGURE 25

The comparison sphere features an average sphere wall reflectance that is constant, a function of each material reflectance. In a single beam instrument, the sphere can be rotated to alternately position each material in the incident beam. In double beam reflectometers, a baseline is initially established with a standard reference material mounted at the sample port opening in order to determine the ratio of incident flux in each beam.

Substitution error also applies to transmittance measurements since the sample surface tangential to the port opening will contribute to the average reflectance of the sphere cavity. A comparison sphere is recommended for transmittance measurements as well.

### 3.2.2 Measurement Geometry $0^\circ/d$ vs. $d/0^\circ$

The previous examples of reflectance and transmittance geometries depicted a directional incident flux and hemispherical collection by the integrating sphere after interaction with the sample material. The geometry is correctly defined as directional/hemispherical and commonly abbreviated as  $0^\circ/d$  referring to near normal incidence and diffuse collection. The  $0^\circ$  angle should be replaced by the actual angle of incidence when describing a particular integrating sphere instrument, for example,  $8^\circ/d$ . Reflectance factor is the quantity directly measured in  $0^\circ/d$  geometry.

A reciprocal optical geometry can be used in both reflectance and transmittance measurements. In the  $d/0^\circ$  geometry, the sample irradiation is hemispherical and the sample is viewed from the near normal direction.

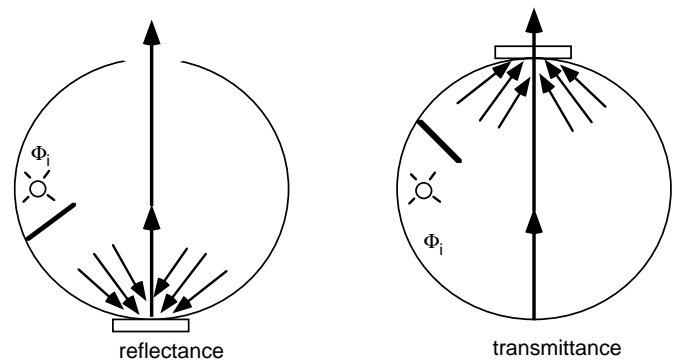


FIGURE 26

The measurement quantity in the reflectance geometry is properly termed the *radiance factor*. The radiance of the sample under diffuse irradiation is compared to the radiance of a reference material. The radiance factor is equivalent to the reflectance factor for reciprocal geometries, i.e.- the étendue and angle from the sample normal is the same for the directional beams, a hemispherical detector field-of-view ( $0^\circ/d$ ) is replaced by a hemispherical input flux ( $d/0^\circ$ ). Instruments which use  $d/0^\circ$  often employ an auxiliary integrating sphere source.

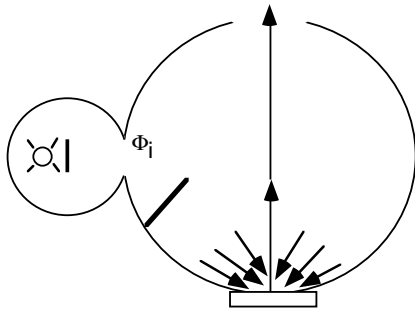


FIGURE 27

There are two main advantages of the  $d/0^\circ$  geometry. The incident flux is significantly greater since integrating spheres provide total light collection, thus increasing the signal-to-noise ratio for the instrument. Polychromatic irradiation will stimulate photon induced radiance, such as that due to fluorescence, which often needs to be quantified in many color and appearance measurements. The main disadvantage of  $d/0^\circ$  instruments is sample heating which can induce thermochromic effects. Many commercial color measurement instruments will utilize flashlamps to reduce thermal measurement error.

### 3.3 Uniform Sources

In the previous applications, the integrating sphere is used as a collecting device for the measurement of radiant flux, either the absolute amount emitted from a light source itself or the relative amount of flux transmitted or reflected by materials.

The open port of an internally illuminated integrating sphere can itself serve as a large area diffuse light source.

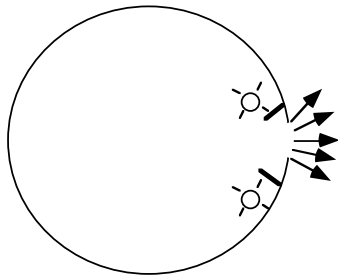


FIGURE 28

Lamps are placed inside the integrating sphere around the perimeter of the viewing port. The lamps are usually baffled from the port. The radiance of the sphere is a function of the wattage rating of the lamp. Multiple lamps can be used

to increase the radiance as well as provide a step wise method of attenuating the radiance level.

Tungsten halogen lamps are most commonly used with integrating sphere sources. These lamps provide a continuous spectrum, free of emission lines or temporal instability when operated from a current regulated power supply. The spectral radiance of the sphere source can be estimated by combining the sphere radiance equation with blackbody equations for the spectral radiant flux.

$$L_{s\lambda} = \frac{\Phi_{i\lambda}}{\pi A_s} \cdot \frac{\rho(\lambda)}{1 - \rho(\lambda)(1 - f)} \quad \text{EQ. 31}$$

and,

$$\Phi_{i\lambda} = \frac{\Phi_0}{\sigma T^4} \cdot \frac{c_1}{\lambda^5} \cdot \frac{1}{(\exp(c_2/\lambda T) - 1)} \quad \text{EQ. 32}$$

where;

$\rho(\lambda)$  = spectral reflectance of sphere surface

$\Phi_{i\lambda}$  = spectral radiant flux

$\Phi_0$  = rated wattage of the lamp

$\lambda$  = wavelength

$T$  = temperature of the filament

$\approx$  correlated color temperature

$c_1, c_2, \sigma$  = blackbody constants

The radiance equation is multiplied by the number of lamps if more than one lamp is used.



3.3.1 Modifying the Source Radiance

If it is required to either modify the spectral radiance or provide greater adjustability in radiance level, then the lamp must be placed externally to another port opening.

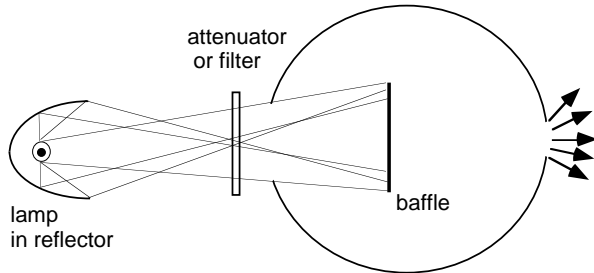


FIGURE 29

The incident radiant flux is modified by the efficiency of the optics used. The centrally located baffle is recommended. Direct illumination through a side port would create areas of increased radiance. The field of view into the integrating sphere should be confined to the baffle. The sphere surface surrounding the baffle tends to be more brightly illuminated. If an optical filter is used to shape the spectral radiance, care should be taken to ensure that the focused light from the reflector does not damage the filter.

When the field-of-view must be wider than the baffle will permit, a diffuse input at an entrance port opening adjacent to the viewing port can be provided by an auxiliary integrating sphere.

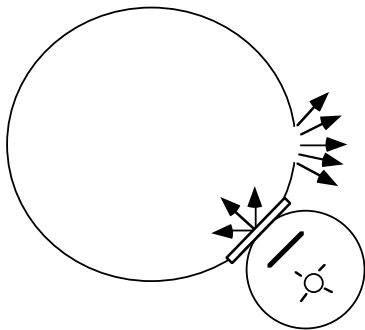


FIGURE 30

In this case, the distance between spheres should be minimized or the incident illumination becomes more directional than diffuse. The system in Figure 29 is more efficient than the auxiliary sphere design for a single lamp. Multiple auxiliary sphere inputs can be considered to increase the radiance of the larger sphere.

3.3.2 Irradiance Uniformity

*Radiance* is the flux density leaving a radiant surface as viewed from a distance away from the surface. A *Lambertian* surface features a radiance that is perfectly diffuse, independent of viewing angle. *Irradiance* is the flux density falling on a surface and is measured at the plane of the surface.

Integrating sphere sources are most often used to test an imaging system. The desired effect is uniform radiance within the field-of-view of the system under test.

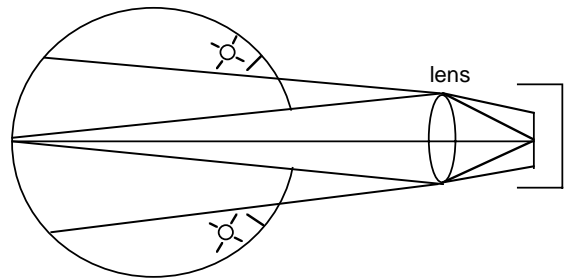


FIGURE 31

The source can be used to back illuminate a printed or etched image such as photographic film for image digitization or resolution targets for MTF testing. Radiance uniformity to within 1%-2% is ensured by using one of the three designs previously illustrated.

It is sometimes desired to use the sphere source for testing a non-imaging device such as a CCD or similar array detector. In this case the desired effect is uniform irradiance. The device under test is often placed coaxial with, but at some distance away from the port of the integrating sphere source. When used in this way, the two important quantities to be determined are the axial irradiance at the center of the object as well as the irradiance at the off-axis edge.

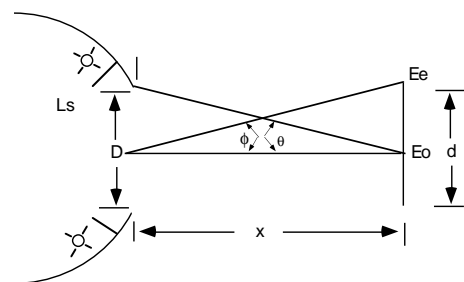


FIGURE 32

# INTEGRATING SPHERE THEORY AND APPLICATIONS

In Figure 32, the axial illuminance,  $E_0$  is given by:

$$E_0 = \pi L_s \sin^2 \theta \quad \text{EQ. 33}$$

Even for a perfectly Lambertian, perfectly uniform circular source, the uniformity of the irradiance across a plane object at a finite distance will vary with the off-axis angle  $\phi$ . The uniformity fall off is given in Table 1 where both the distance and the dimension of the object are expressed as multiples of the sphere port diameter,  $x/D$  and  $d/D$  respectively. Uniformity is defined as the ratio of the irradiance at the edge of the object to the axial irradiance,  $E_e/E_0$ .

Examination of Table 1 reveals that the uniformity is 100% at the plane of the port. It decreases as the object is moved away from the port for a short distance and improves as the distance becomes sufficiently long. This phenomenon can be illustrated graphically as shown in Figure 33.

For small values of both  $\theta$  and  $\phi$  ( $<10^\circ$ ), the irradiance at the edge is given by the commonly used *cos<sup>4</sup>φ law of illumination* where:

$$E_e = E_0 \cos^4 \phi \quad \text{EQ. 34}$$

In the examples illustrated Sfor a source diameter equal to or larger than the object, the  $\cos^4 \phi$  law predicts the edge irradiance to within 1% for source to object distances at least two times larger than the source diameter. At this distance, the uniformity is within 10%, however, the irradiance is less than 5% of the value at the plane of the port.

It is important to note that Table 1 and Figure 33 display calculated theoretical values of uniformity for the ideal perfectly Lambertian source. Laboratory measurements of real integrating sphere sources correlate extremely well with these predicted values. Therefore, the data provided can be used as design guidelines in choosing the correct uniform source for a particular application.

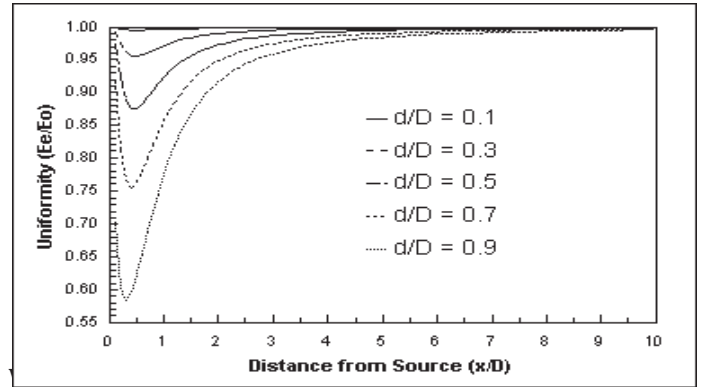


FIGURE 33

TABLE 1

Object Diameter d/D	Irradiance Uniformity ( $E_e/E_0$ ) Distance from Source ( $x/D$ )												
	0.00	0.10	0.20	0.25	0.50	0.75	1.00	1.50	2.00	2.50	3.00	5.00	10.00
0.1	1.00	1.00	1.00	1.00	1.00	1.00	1.00	1.00	1.00	1.00	1.00	1.00	1.00
0.2	1.00	1.00	0.99	0.99	0.98	0.98	0.99	0.99	1.00	1.00	1.00	1.00	1.00
0.3	1.00	0.99	0.98	0.97	0.96	0.96	0.97	0.98	0.99	0.99	1.00	1.00	1.00
0.4	1.00	0.99	0.96	0.94	0.92	0.93	0.95	0.97	0.98	0.99	0.99	1.00	1.00
0.5	1.00	0.97	0.92	0.90	0.88	0.90	0.92	0.96	0.97	0.98	0.99	1.00	1.00
0.6	1.00	0.95	0.88	0.85	0.82	0.86	0.89	0.94	0.96	0.97	0.98	0.99	1.00
0.7	1.00	0.92	0.81	0.78	0.76	0.81	0.86	0.92	0.95	0.96	0.97	0.99	1.00
0.8	1.00	0.84	0.72	0.69	0.70	0.76	0.82	0.89	0.93	0.95	0.97	0.99	1.00
0.9	1.00	0.70	0.60	0.59	0.62	0.71	0.78	0.87	0.92	0.94	0.96	0.98	1.00
$\sin^2 \theta$	1.000	0.962	0.862	0.800	0.500	0.308	0.200	0.100	0.059	0.038	0.027	0.010	0.002
$\pi \sin^2 \theta$	3.142	3.021	3.708	2.513	1.571	0.967	0.628	0.314	0.185	0.121	0.085	0.031	0.008

Note: Boundary lines delineate regions of 98%, 95%, and 90% irradiance uniformity

# GUIDE TO OPTICAL UNITS

## PHOTOMETRIC QUANTITIES AND UNITS

Quantity	Symbol	Units	Abbreviations
Luminous energy	$Q_v$	Lumen•second $\equiv$ talbot	lm•s $\equiv$ talbot
Luminous density	$U_v$	Lumen•second/m <sup>3</sup>	lm•s/m <sup>3</sup>
Luminous flux	$\Phi_v$	Lumen	lm
Luminous efficacy	K	lumen/watt	lm W <sup>-1</sup>
Luminous exitance	$M_v$	lumen/m <sup>2</sup>	lm m <sup>-2</sup>
Luminance (brightness)	$L_v$	candela/m <sup>2</sup> candela/ $\pi$ ft <sup>2</sup> $\equiv$ footlambert candela/ $\pi$ cm <sup>2</sup> $\equiv$ lambert	cd/m <sup>2</sup> cd/ $\pi$ ft <sup>2</sup> $\equiv$ fL cd/ $\pi$ cm <sup>2</sup> $\equiv$ L
Luminous intensity	$I_v$	candela	cd (lm sr <sup>-1</sup> )
Illuminance	$E_v$	lumen/m <sup>2</sup> $\equiv$ lux lumen/ft <sup>2</sup> $\equiv$ footcandle	lm/m <sup>2</sup> $\equiv$ lx lm/ft <sup>2</sup> $\equiv$ fc

## RADIOMETRIC QUANTITIES AND UNITS

Quantity	Symbol	Units	Abbreviations
Radiant energy	Q	joule $\equiv$ watt-second	J $\equiv$ W•s
Radiant energy density	U	joule/m <sup>3</sup>	J/m <sup>3</sup>
Radiant flux (power)	$\Phi, P$	watts $\equiv$ joule/second	W $\equiv$ J/s
Radiant exitance	M	watts/m <sup>2</sup>	W/m <sup>2</sup>
Radiance	L	watts/m <sup>2</sup> •steradian	W/m <sup>2</sup> •sr
Radiant intensity	I	watts/steradian	W/sr
Irradiance	E	watts/m <sup>2</sup>	W/m <sup>2</sup>

## SPECTRAL RESPONSE OF THE NORMAL HUMAN EYE WITH LUMINOUS TO RADIOMETRIC CONVERSION

Wavelength (nm)	CIE Photopic Luminous Efficiency Coefficient	Photopic Lumen/Watt Conversion Factor	Wavelength (nm)	CIE Photopic Luminous Efficiency Coefficient	Photopic Lumen/Watt Conversion Factor
390	0.0001	0.13	570	0.9520	649.0
400	0.0004	0.27	580	0.8700	593.0
410	0.0012	0.82	590	0.7570	516.0
420	0.0040	2.73	600	0.6310	430.0
430	0.0116	7.91	610	0.5030	343.0
440	0.0230	15.7	620	0.3810	260.0
450	0.0380	25.9	630	0.2650	181.0
460	0.0600	40.9	640	0.1750	119.0
470	0.0910	62.1	650	0.1070	73.0
480	0.1390	94.8	660	0.0610	41.4
490	0.2080	142.0	680	0.0170	11.6
500	0.3230	220.0	670	0.0320	21.8
510	0.5030	343.0	690	0.0082	5.59
520	0.7100	484.0	700	0.0041	2.78
530	0.8620	588.0	710	0.0021	1.43
540	0.9540	650.0	720	0.0010	0.716
550	0.9950	679.0	730	0.0005	0.355
555	1.0000	683.0	740	0.0003	0.170
560	0.9950	679.0	750	0.0001	0.820